A&A 485, 435–449 (2008)
DOI: 10.1051/0004-6361:20078119

Astronomy & Astrophysics

BVRI photometric analysis for the galaxy group NGC 4410

J. A. Pérez Grana[1,2], S. N. Kemp[1,2], A. C. Katsiyannis[3,4], A. Franco-Balderas[5], E. de la Fuente[1,2], J. Meaburn[6,7], and H. G. Khosroshahi[8]

[1] Departamento de Física, CUCEI, Universidad de Guadalajara, Avenida Revolución SN, Guadalajara, Jalisco, México
[2] Instituto de Astronomía y Meteorología, Universidad de Guadalajara, Avenida Vallarta No. 2602, Col. Arcos Vallarta, CP 44130, Guadalajara, Jalisco, México
e-mail: arturopg@astro.iam.udg.mx
[3] Institute of Astronomy and Astrophysics, National Observatory of Athens, I. Metaxa & V. Paulou, Penteli, 15236 Athens, Greece
[4] Royal Observatory of Belgium, Solar Physics, Ringlaan 3, 1180 Brussels, Belgium
[5] Instituto de Astronomía, Universidad Nacional Autónoma de México, Apartado Postal 70-264, 04510, México DF, México
[6] Instituto de Astronomía, Universidad Nacional Autónoma de México, CP 22800, Ensenada, Baja California, México
[7] Jodrell Bank Observatory, School of Physics and Astronomy, University of Manchester, Macclesfield, Cheshire, SK11 9DL, UK
[8] Astrophysics Research Institute, Liverpool John Moores University, 12 Quays House, Egerton Wharf, Birkenhead, CH41 1LD, UK

Received 19 June 2007 / Accepted 17 March 2008

ABSTRACT

We present a *BVRI* CCD (Charge Coupled Device) surface photometry analysis of the galaxy group NGC 4410, which contains four galaxies in interaction. Along with our photometric study, we show residual images (after subtracting isophotal models) and unsharp masked images to uncover any hidden structures in this system of galaxies; we have also performed a two-dimensional bulge-disk decomposition for NGC 4410C and D, and a major axis sector profile for NGC 4410A. We have calculated *BVRI* surface brightnesses and colors within regions such as galaxy centers, bridges, tails and optical knots in the NGC 4410 system, generating $B-V$ color maps and color profiles. The information obtained was used to discover the predominant stellar populations. The colors of the galaxies imply ages of $\sim 2\times10^9$ to $\sim 2\times10^{10}$ years for models using a range of metallicities. The bluer knots and H II regions have colors implying ages of a minimum of 5×10^8 years, but possibly as high as 3×10^9 years for stellar populations formed in the interaction. These results lead us to conclude that there is a moderate star formation rate and a tranquil evolving state of the system with a long timescale for interaction, much longer than the typical dynamical timescales of 10^8 years. Although we note that NGC 4410D has a blue nucleus (possible nuclear starburst?), bulge, bar, and short spiral arms, and may be interacting with a H I gas cloud. Some observed structures in NGC 4410A are coincident with previously studied H II regions, a tidal arm and optical/radio knots found in this galaxy. An optical knot E coincident with a radio knot may be an optical synchrotron emission or an H II region. The galaxy NGC 4410B appears to be a boxy giant elliptical with a possible dusty disk embedded (similar to Cen A?) and NGC 4410C is confirmed as a lenticular galaxy.

Key words. galaxies: photometry – galaxies: interactions – galaxies: evolution – galaxies: individual: NGC 4410

1. Introduction

The group of galaxies NGC 4410 is a peculiar group of twelve galaxies with velocities in the range 6900−7500 km s^{-1} (Smith 2000) with four components in obvious interaction: NGC 4410 A-D (Figs. 1–3). This group lies at a distance of 97 Mpc (using $H_0 = 75$ km s^{-1} Mpc^{-1}, which gives a scale of $1'' = 470$ pc) and is of particular interest for having prominent optical bridges and filaments as well as different galaxy types, which could represent a particular phase in the formation of an elliptical galaxy from the slow merger of members of a group. The galaxy NGC 4410A ($\alpha = 12^h23^m55^s$, $\delta = 09°17'40''$, J2000.0) has been classified as a Sab pec asymmetric double-lobed radio-galaxy (Hummel et al. 1986; Tschöcke et al. 1999; Smith 2000), with the radio emission interpreted as a distorted radio jet. This galaxy forms a galaxy pair and, most probably, a future merger (Smith 2000; Donahue et al. 2002; Smith et al. 2003) with the E? pec or S0? pec galaxy (Hummel et al. 1986; Smith 2000) NGC 4410B. This galaxy pair (NGC 4410A/B) has two diffuse optical filaments, one at the NW of NGC 4410A and the other at SE of NGC 4410B (Hummel et al. 1986; Smith 2000), and a tidal bridge connecting with NGC 4410C, a S0? type (Smith 2000). In this galaxy pair, there are some optical knots visible in our color maps situated near the NGC 4410A nucleus and classified as H II regions (Donahue et al. 2002). Two more optical and radio knots in the southeast tail of NGC 4410A/B (knots E and F identified by Hummel et al. 1986; and mentioned by Donahue et al. 2002) are also visible in our CCD fields. The four galaxies are connected by two optical bridges; one, previously mentioned, connects NGC 4410A/B and NGC 4410C, while the second bridge connects NGC 4410C with NGC 4410D, a SBa type galaxy with a prominent, distorted bar (Hummel et al. 1986).

Here, we apply similar techniques to those used in our photometric and morphological study of ESO 383–45 (Kemp et al. 2005), a galaxy that may be undergoing ram-pressure stripping or may be a merger remnant. In this previous paper (Kemp et al. 2005), we used digitally co-added Schmidt telescope data and multicolor CCD photometry to produce color maps and surface brightness and color profiles, as well as unsharp masked and self-correlated images. We have previously published images of the NGC 4410 group at varying contrast levels (Katsiyannis et al. 2001; Kemp et al. 2002) extracted from a co-added array

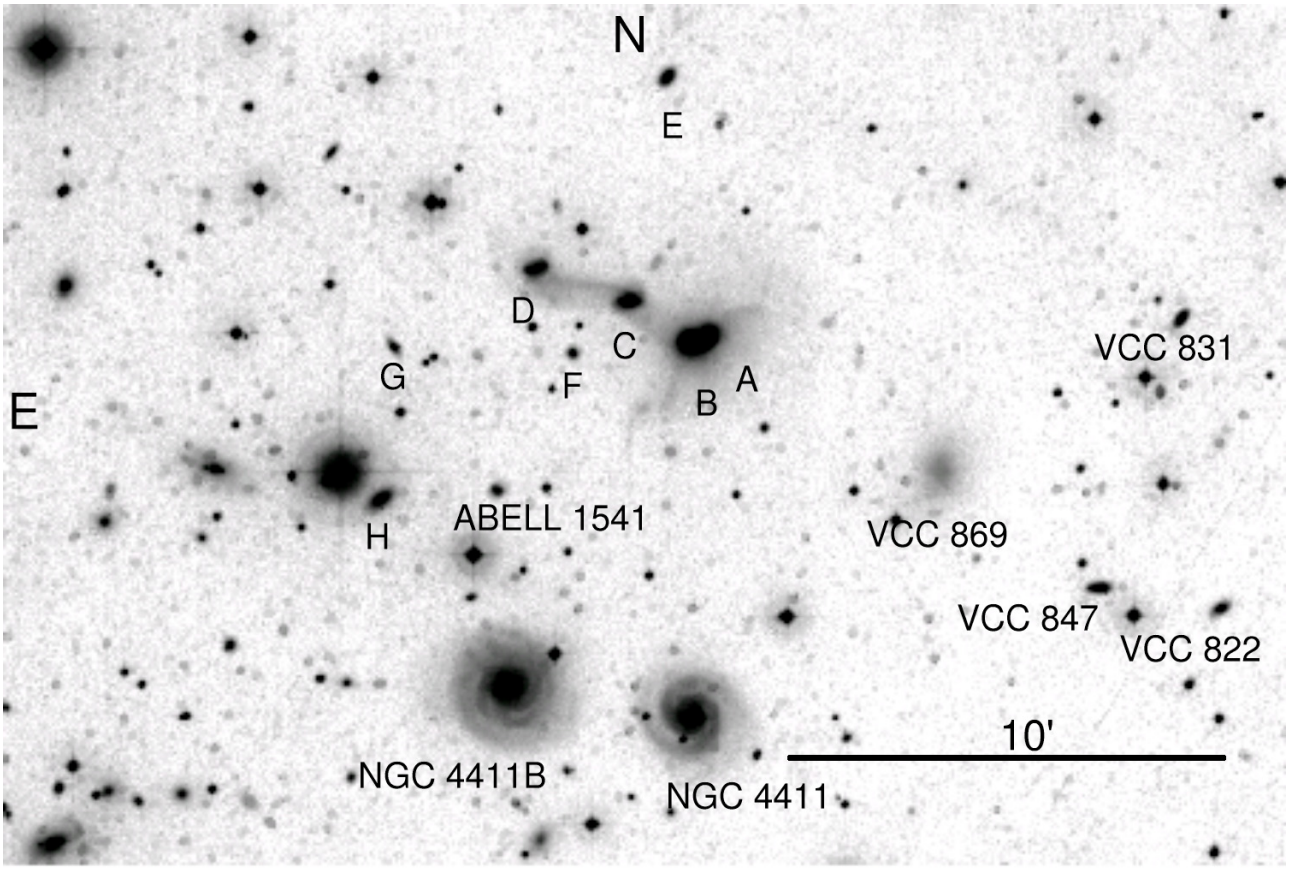

Fig. 1. Field containing 11 of the 12 confirmed members of the NGC 4410 group. Letters from A to H, and K refer to NGC 4410A, NGC 4410B, etc. (FGC 170A, the 12th confirmed member, lies to the north of this field). The naming of the group members is as used in Smith (2000). NGC 4410A has coordinates $\alpha = 12^{h}23^{m}55^{s}$, $\delta = 09°17'40''$ (J2000.0). The directions North and East are indicated. The image is part of the co-addition of digital scans of 13 Kodak Tech-Pan Schmidt films (Katsiyannis et al. 1998).

of 13 digitally-scanned Kodak Technical Pan films of the NE region of the Virgo cluster, taken with the UK Schmidt Telescope. In these digitally co-added Schmidt films, the NGC 4410 group stands out as an interacting group of distinctive, if not unique, appearance, and worthy of further study (and with relatively few previous studies published in the literature).

Previous studies of the NGC 4410 group suggest that a multicolor surface brightness analysis should be carried out to corroborate facts such as the moderate star formation of 1−4 $M_{\odot}$ yr^{-1} in the H II regions of NGC 4410A and the existence of optical knots (Hummel et al. 1986) and H II regions (Donahue et al. 2002). Also, it is necessary to investigate the relation between structures seen in CO, 21 cm and 20 cm observations (Smith 2000) and to obtain the dominant stellar spectral colors (stellar populations). Using color photometry and residual images, we have found optical counterparts for structures detected in previous studies and images that could indicate the presence of internal structures.

In Sect. 2, we describe the vaious observational datasets and the procedures used in the data reduction and analysis. In Sect. 3, the results are given for each galaxy in turn. In Sect. 4, we discuss the implication of these results for the stellar populations in each galaxy, and review the morphological types of each member and the evidence for internal structures. In Sect. 5, we provide a summary and conclusions.

2. Observations and data reduction

Our data includes a section from a stack of 13 digitally co-added Schmidt films, and three observational periods of direct optical imaging from three different telescopes.

2.1. The Schmidt films

The use of digitally co-added Schmidt material has been shown to be a powerful technique for the detection of low surface brightness material in groups and clusters of galaxies (see Kemp & Meaburn 1993). We have a data array of 13 digitally co-added Tech-Pan films obtained with the UK Schmidt Telescope (Katsiyannis et al. 1998, 2001; Kemp et al. 2002) from which we show a region containing 11 members of the NGC 4410 group (Fig. 1) and the four interacting members of the group (Fig. 2). The pixel size of the scans is 2″×2″. Using the Extended Surface Photometry (ESP)[1] *skew* task (Gray et al. 2000), we produced an image that enhanced faint diffuse objects (Fig. 3). This program produces an image of the field in which each pixel value represents the extent to which the count values surrounding this pixel are not distributed in a Gaussian manner (i.e., the skewness of the local distribution of pixel values). The influence of bright objects or cosmic rays is reduced by applying a threshold pixel value (a number of standard deviations above sky level) where

[1] The ESP package is part of the Starlink software package distributed by the Rutherford Appleton Lab.

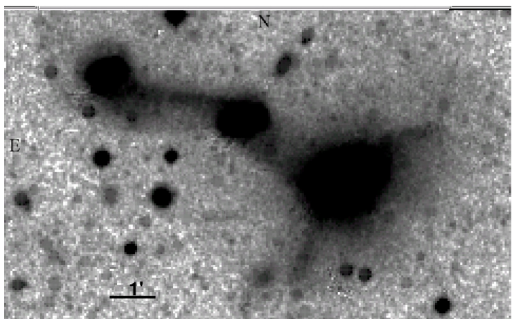

Fig. 2. A high contrast image of the four interacting components in the NGC 4410 group from the digitally co-added Schmidt Tech-Pan films.

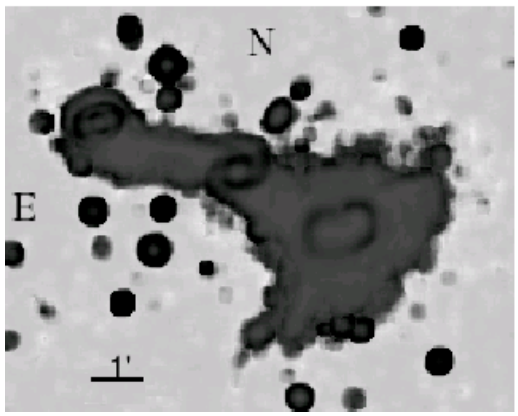

Fig. 3. A skewness representation of the NGC 4410 group showing the extent of faint diffuse matter.

any pixel found above that value is ignored. The skewness value assigned to each pixel of the output image is calculated using the values of pixel counts found for all the non-bad pixels.

2.2. The 1 m Jacobus Kapteyn telescope

Our first CCD direct imaging observations of the NGC 4410 group were carried out on 1999 February 16 with the 1 m Jacobus Kapteyn Telescope (*JKT*) in the Observatorio del Roque de los Muchachos (La Palma). We observed using a set of *BVRI* filters on the Harris system with the Tek1 CCD camera having a scale of 0.33″ pixel^{-1} and a CCD field of view of 5.6′ × 5.6′ with a seeing of 1″. We took one exposure of 45 min in *B* and one exposure of 30 min in each of *V*, *R*, and *I*. Sky brightnesses during these observations were $\mu_{B,\mathrm{sky}} \approx 22.0$ mag arcsec^{-2} and $\mu_{R,\mathrm{sky}} \approx 20.0$ mag arcsec^{-2}.

2.3. The 0.84 m San Pedro Mártir telescope

During 2001 April 23 to May 1, we carried out more observations with the 0.84 m telescope at the Observatorio Astronómico Nacional, San Pedro Mártir (SPM) Baja California, México. We used two different CCD's: the SITe2 and the Thomson2k. The newly-acquired SITe2 was the only CCD available at the beginning of the run. We used the Thomson 2k for the blue images when it became available as it is more sensitive in *B*. We used the *BRI* filters of the Johnson-Cousins system. In order to obtain a better signal-to-noise ratio (obtaining a good image for faint light structures such as bridges and tails), we produced a 3 h image by combining individual *B* exposures of 30 min. We used a 2 × 2 pixel pre-binning which produces a 1024 × 1024 pixel image with the Thomson2k, with a scale of 0.532″ pixel^{-1} and field of view of 9.1′ × 9.1′. The typical seeing for the *B* images was very poor, ∼4″. With SITe2, we obtained 1.16 h combined images in both *R* and *I*, with a 0.421″ pixel^{-1} scale, field of view of 7.2′ × 7.2′ with a typical seeing of 3″. The images obtained contained some reflections mainly attributed to the mirrors of the autoguider and to the baffles in the telescope as well as some background structure in the SITe2 chip. We were able to model one of the reflections (due to the baffles) and then subtract the model so this reflection had a reduced effect on the photometry of the galaxies. We generated this model by combining (in each filter) images that contain the reflection, and zero or few objects. The model image was subtracted from the object images, smoothing the model image when necessary to improve the resultant image. Still, we had some reflections that could not be modeled and affected the photometry of the filaments in NGC 4410A/B. This effect was reduced by measuring and subtracting a local sky background value for each filament, while measuring the surface brightness of the filament. Sky brightnesses during these observations were $\mu_{B,\mathrm{sky}} \sim 21.8$ mag arcsec^{-2} and $\mu_{R,\mathrm{sky}} \sim 19.8$ mag arcsec^{-2}.

2.4. The 2.1 m SPM telescope

The final observational run was carried out during 2004 April 9−12 with the 2.1 m SPM telescope. The SITe3 CCD camera with the *BVRI* Johnson filters in the Italian filter wheel were used. We obtained total combined exposure times of 2.5, 1.5, 1, 0.5 h in *BVRI* respectively, and a 70 min total exposure for onband Hα (λ_0 = 6723 Å, $\Delta\lambda$ = 80 Å) and 40 min total exposure for offband (λ_0 = 6643 Å, $\Delta\lambda$ = 80 Å). After sky subtraction we used the three brightest stars in the field to determine the ratio of transmission through the on-band and off-band filters. The off-band image was scaled according to this ratio and subtracted from the on-band image. The scale for this data was 0.31″ pixel^{-1} and the CCD field of view was 5.1′ × 5.1′ with a typical seeing of ∼3″. Sky brightnesses during these observations were $\mu_{B,\mathrm{sky}} \sim 21.4$ mag arcsec^{-2} and $\mu_{R,\mathrm{sky}} \sim 19.5$ mag arcsec^{-2}.

2.5. The HST image

We used a Hubble Space Telescope (HST) public image of NGC 4410A. The image is a 8.3 min exposure with the broadband filter centered at λ_0 = 5934 Å, taken with the Wide Field Planetarie Camera 2 (WFPC2) which has 800 × 800 pixels of 0.045″ × 0.045″.

2.6. Data reduction

Bias subtraction, dark current correction, and flat fielding of the images were carried out using standard techniques in the Image Reduction and Analysis Facility (IRAF)[2]. In each run, observations of Landolt standard fields containing Palomar Green stars (Landolt 1992) were performed during the night at a range of airmasses. Instrumental magnitudes were obtained using IRAF's *phot* task. Estimates of the extinction coefficients were obtained by plotting instrumental magnitudes against airmass for multiple observations of the same field of standard stars, and these

[2] IRAF is distributed by the National Optical Astronomy Observatory which is operated by AURA, Inc., under contract with the NSF.

estimates of the extinction coefficients were used to derive values for the photometric zero points and color terms. Using the standard format for the linear calibration equation:

$$m_s = m_I + C_0 + C_1 X + C_2 \text{stdcol}; \quad (1)$$

m_s: standard catalog magnitude of the object,
m_I: instrumental magnitude of the object,
C_0: photometric zero point,
C_1: extinction coefficient,
X: effective airmass,
C_2: color term,
stdcol: color index.

Our resulting equations are:

1 m *JKT* Telescope (La Palma) 1999 February 16:

$$B = b + 22.83 + 0.21X + 0.06(B - V)$$
$$V = v + 22.89 + 0.12X + 0.03(B - V)$$
$$R = r + 23.04 + 0.08X + 0.03(V - R)$$
$$I = i + 22.44 + 0.05X + 0.08(V - I)$$

0.84 m Telescope (SPM) 2001 April 23 to May 1:

$$B = b + 21.13 + 0.19X + 0.06(B - V)$$
$$R = r + 21.71 + 0.06X + 0.03(R - I)$$
$$I = i + 21.53 + 0.03X + 0.05(R - I)$$

2.1 m Telescope (SPM) 2004 April 9–10:

$$B = b + 23.29 + 0.31X + 0.13(B - V)$$
$$V = v + 24.43 + 0.22X + 0.04(B - V)$$
$$R = r + 24.64 + 0.15X + 0.02(V - R)$$
$$I = i + 24.09 + 0.10X + 0.01(V - I).$$

We note that with the 2.1 m data we have used Landolt standards, which are defined in the Johnson-Kron-Cousins system, while the filters in the Italian filter wheel correspond to the Johnson filters, and in the R and I bands there are significant differences between the two filter systems. We compared the radial brightness profiles of galaxies NGC 4410C and NGC 4410D between the *JKT* and the 2.1 m SPM data and found no significant differences in their R and I band surface brightnesses at corresponding radii, although NGC 4410D in particular has a wide variation of color with radius. Observations of other galaxies for which we have data taken with the Johnson-Cousins filters and the Johnson filters (calibrated also using Landolt standards) also show no systematic trend between the resulting surface brightness profiles. It seems that at most we have errors of ±10%, hence we found no problems in using the Johnson filters with Landolt stars and comparing the R and I surface brightnesses obtained with the results of other Johnson-Cousins photometry. We also note that the extinction coefficients are somewhat higher for the nights of 2004 April 9–10 in the 2.1 m due probably to the high winds and atmospheric turbulence of those nights, which also had poor seeing (~3″).

For the 0.84 m telescope, although we minimized the effect of reflections by modeling and subtracting the reflection due to the baffles of the telescope, other reflections (e.g. due to the autoguider mirror position) plus some residual background with the SITe2 chip (R and I filters) remain. We do not include quantitative results for the fainter parts of the galaxies for this telescope, although we include the 0.84 m telescope calibration equations here. We confirmed that the surface brightnesses of the central regions of the galaxies are the same in the 0.84 m data as in the other telescopes within the error margin, and taking into account differences in seeing.

Images from the same telescope were corrected for seeing variations and then aligned using 10 stars in each field with the IRAF programs *geomap* and *geotran*. Star and galaxy images were separated according to the object FWHM and the stars were removed from the images by interpolating from neighboring background values around a circular aperture. We produced a final image for each filter by combining the individual aligned images (corrected for extinction), and we applied the calibration equations to this image to generate calibrated images in each filter in which the pixel values correspond to the surface brightness values of the galaxies at that position. Color maps were generated by subtraction of these calibrated images.

We performed surface photometry was performed on the galaxies using the final images in counts with the stars removed. We generated radial color profiles by subtraction of the individual calibrated surface brightness profiles. Corrections for Galactic extinction correspond to $A_B \sim 0.0$ (Donahue et al. 2002) and to a magnitude value of 0.01 for redshift K corrections (Sparke & Gallagher 2000). In both cases the correction was negligible.

The inclination angle for each galaxy was calculated by using Holmberg's formula (see Chiba & Yoshi 1995)

$$\cos^2 i = \frac{q^2 - q_0^2}{1 - q_0^2}, \quad (2)$$

where q is the axial ratio defined as $q = b/a$, (b, a being the semi-minor and semi-major axis of the galaxy at an isophote of 25 mag arcsec^{-2} in B) and q_0 is fixed to be 0.2.

We calculated apparent magnitudes by measuring the total flux in each galaxy within the isophote that corresponds to 25.6 mag arcsec^{-2} in B, by using the *ellipse* and *polyphot* task in *IRAF* to have elliptical and polygonal apertures. Absolute magnitudes were calculated using a distance of 97 Mpc to the group. The average colors for each galaxy were obtained by subtraction of the relevant total magnitudes.

We calculated corrections for internal extinction for the total magnitudes and colors of the disk galaxies by using the formula for the inclination-dependent extinction in the B-band A_B^i described by Tully & Fouqué (1985; also see Matthews et al. 1998; Pierini 1999), i.e.:

$$A_B^i = -2.5\log\left[f(1 + e^{-\tau \sec i}) + (1 - 2f)\left(\frac{1 - e^{-\tau \sec i}}{\tau \sec i}\right)\right], \quad (3)$$

where i is the inclination angle of the galaxy, $\tau = 0.55$ is the optical depth, and $f = 0.25$ is the fraction of light in front of the sheet of finite thickness in which the whole absorption occurs. Given that Tully & Fouqué note that the absolute correction A_B^i is poorly defined but the correction to face-on orientation, $A_B^{i-0} = A_B^i - A_B^0$ is better defined, we report corrections to face-on orientations only in the results here. Corrections for other filters are calculated using the standard interstellar extinction law (Rieke & Lebofsky 1985). The surface brightness profiles reported in Sect. 3 have not had the internal extinction corrections applied.

We carried out further morphological classification using 2D surface brightness fitting. We attemped to decompose the galaxies into bulge and disk components by fitting a Sersic (1968) profile to the bulge and an exponential profile to the disk. We quantified the morphology of galaxies by the bulge-to-disk ratio, as described in Khosroshahi et al. (2000). For instance, a pure elliptical galaxy (no disk) is judged by a very small disk-to-total luminosity ratio ($D/T < 0.05$), while a pure disk galaxy by $D/T > 0.95$.

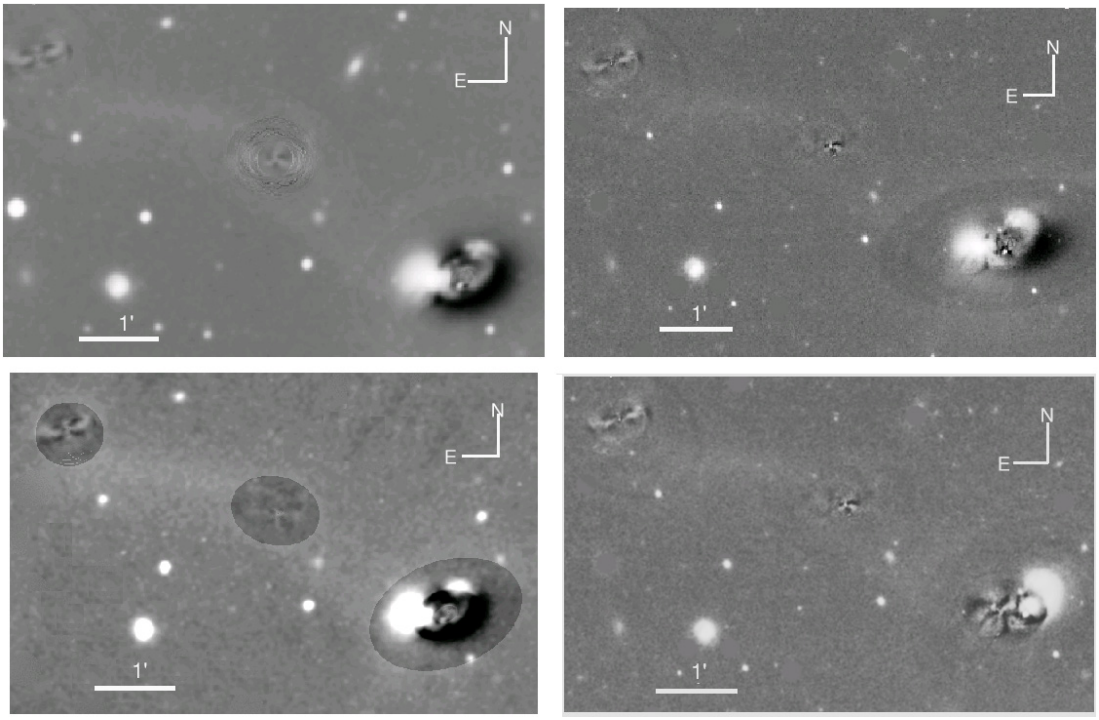

Fig. 4. Residual images of the galaxy group components NGC 4410A, C, D from *B* images from: **a)** the 2.1 m telescope; **b)** the Jacobus Kapteyn (1 m) Telescope; **c)** the 0.84 m telescope; and **d)** a residual *B* image of NGC 4410B,C,D from the 1 m *JKT* telescope. The residual image of NGC 4410A shows possible "spiral arm-like" asymmetrical structures near the nucleus. NGC 4410D shows a prominent bar distorted by the group interaction in all four images.

This procedure was only successful in the cases of NGC 4410C and NGC 4410D, A and B already being in an advanced stage of the process of merging. In any case, given the high level of interaction between the galaxies of the group, and the asymmetry caused as a result of such interaction, we treat the classification with caution as these galaxies are undoubtedly far from being symmetric and smooth. However, we believe this is a useful exercise.

2.7. Residual and unsharp-masked images

Ellipse fitting was carried out using the program *ellipse* in the IRAF *isophote* package and starts from the isophote corresponding to 25.6 mag arcsec^{-2} in *B* (2% of sky level). The best fit isophotal models generated can be subtracted from the final reduced image (in counts) to produce residual images. These images show asymmetric structures such as spiral arms, bars, H II regions, and other structures that may be hidden in the bright central parts of the galaxy. This process was performed on the images obtained from all three telescopes. In the case of NGC 4410A/B, obviously the two galaxies overlap significantly in their brightness distribution. Here, we first apply a mask to one galaxy, for example NGC 4410B, and perform the ellipse fitting on the other galaxy NGC 4410A using the masked image (the surface brightness profiles of NGC 4410A mentioned in Sect. 2.5, and displayed in Sect. 3, were generated from this masked image). The model of NGC 4410A thus generated can be subtracted from an unmasked reduced image (in counts), giving an image that contains the residual structures of NGC 4410A and the uncontamined image of NGC 4410B. The same procedure was repeated to obtain the residual images and surface photometry of NGC 4410B.

We note that many of the ellipse models of NGC 4410A were unsatisfactory at intermediate and outer radii, as the profile starts to increase in brightness at about 10−15 arcsec, exterior to a ring of dust absorption, and the program *e*llipse does not work for radially-increasing brightness gradients. Outside this radius the position angle and ellipticity of the modeled isophotes tends to remain fixed. Thus, we do not report residual structures of NGC 4410 outside the central region.

In Fig. 4, we compare the results obtained for residual structures of NGC 4410 A,C,D from the three telescopes and also show an image of the residual structures of NGC 4410B obtained using the 0.84 m SPM telescope. We examine the detailed results in Sect. 3, but here we note that for NGC 4410C (evidence of disk) and NGC 4410D (curved bar) the results are similar for the three telescopes. For NGC 4410A, the tidal arm to the NW and knots to the SE (corresponding to H II regions in Donahue et al. 2002) are also present in the images from all three telescopes, but the residual images do not completely agree over the central structure of NGC 4410A. The residual images obtained with the 0.84 m telescope point to the presence of inner spiral arms, while the images obtained with the 1 m *JKT* and 2.1 m telescopes also show a central structure, but it is not as well defined as in the images obtained with the 0.84 m. To consider whether these may be real structures we need to compare and analyze the way in which our isophotal model is generated. In this case, we are producing a Fourier expansion of the original surface brightness (Barazza et al. 2002). This kind of model does not make an accurate reproduction of the galaxy center, especially one under gravitational interaction. Hence, by means of fixing parameters such as the ellipticity, position angle, and semi-major axis of the galaxy, we can obtain an asymmetrical radial pattern that may look like internal structures. An example of this kind of situation can be seen in the interacting galaxy pair

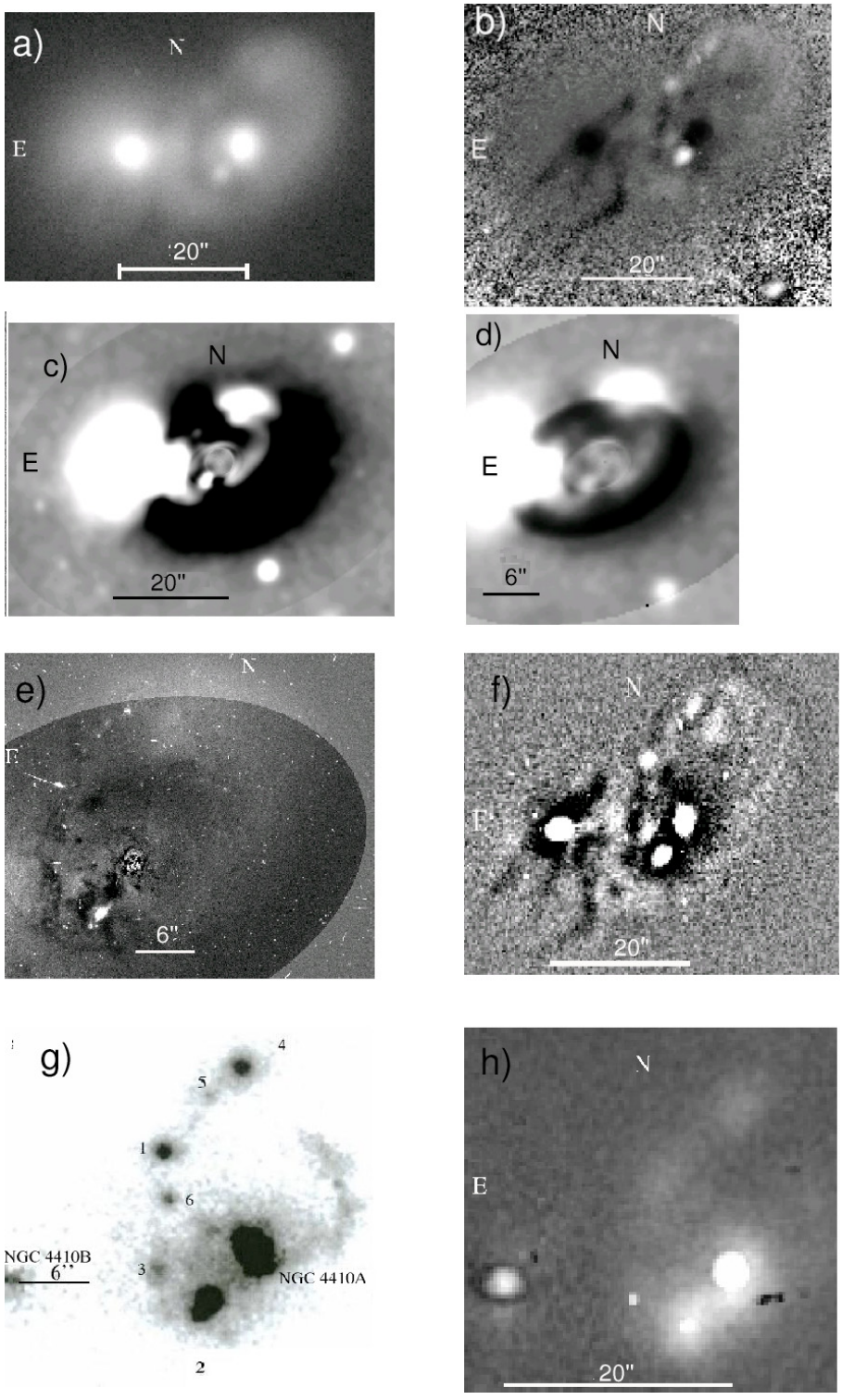

Fig. 5. **a)** NGC 4410A/B in a logarithmic image; **b)** a $(B-V)$ color map image; **c)** a B residual image of NGC 4410A from the 2.1 m telescope; **d)** a B residual image of NGC 4410A from the 0.84 m telescope, in which spiral arms seem to be coincident with some of the H II regions found in this galaxy; **e)** a processed HST public image shows the residual structure of the nucleus of NGC 4410A; **f)** an unsharp masked image in B from the 2.1 m telescope; **g)** the (Hα + [N II]) image of NGC 4410A/B from Donahue et al. (2002); **h)** our (Hα + [N II]) image from the 2.1 m telescope.

IC 829 and MCG-2-33-35 where the subtracted model of IC 829 (a S0 type galaxy) appears to show four radial symmetrical arms (Grützbauch et al. 2005).

Another method for uncovering hidden structures is the unsharp masking method. We use the IRAF Gauss task to smooth the image with a Gaussian function (we use a Gaussian with a value of $\sigma = 3$ pixels) and then subtract this smoothed image from the original generating the "unsharp masked" image. This process was also carried out with the images from all three telescopes.

3. Results

3.1. NGC 4410A/B

Results for NGC 4410A/B are shown in Figs. 4–10 inclusive. We comment on the residual images of NGC 4410A (in B from the three telescopes) and NGC 4410B (in B from the 0.84 m) in Sect. 2.7. In Figs. 5a–h we show various images of NGC 4410A/B. Figure 5a is a B logarithmic image that shows the complicated structures of A (right of center) with its nucleus and small H II region SE of the nucleus (region 2 in

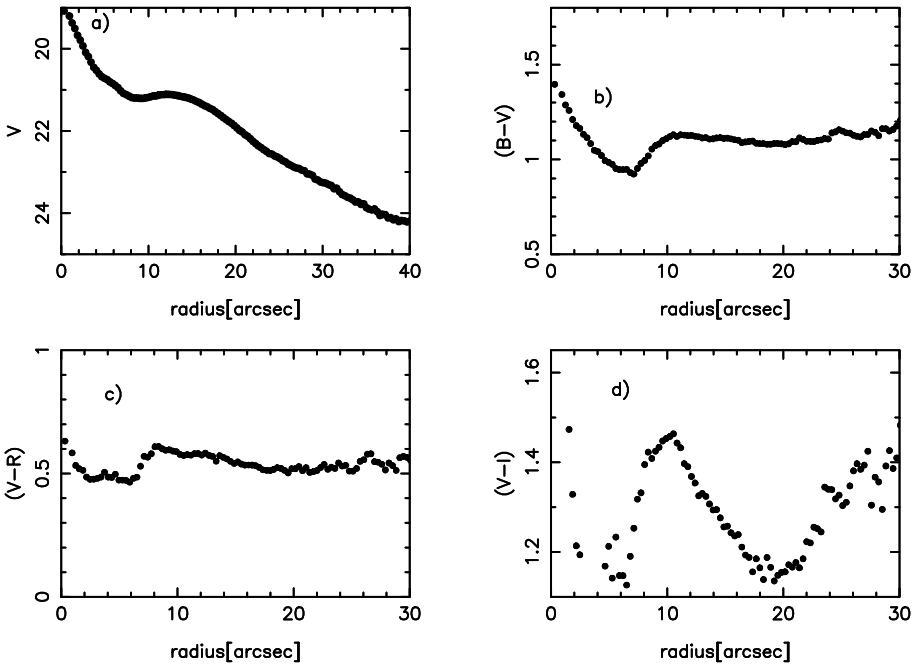

Fig. 6. Surface brightness and color profiles of NGC 4410A **a)** V, **b)** $B-V$, **c)** $V-R$, and **d)** $V-I$. ($1'' = 470$ pc with $H_0 = 75$ km s^{-1} Mpc^{-1}).

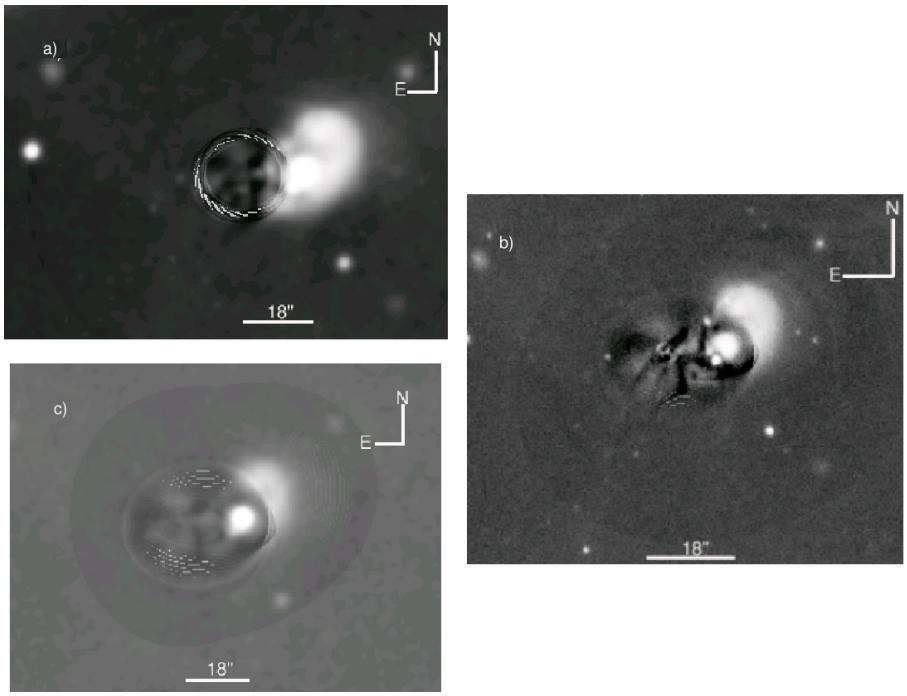

Fig. 7. Residual images of NGC 4410B in B band, **a)** 2.1 m telescope, **b)** 1 m telescope, **c)** 0.84 m telescope.

Donahue et al. 2002) and tidal arm to the W and NW of the nucleus. Dust lane features can also be seen, especially to the E of the nucleus, although the seeing is poor. The nucleus of NGC 4410B lies ∼18″ E of the nucleus of NGC 4410A. Figure 5b is a $B-V$ color map of the same field. Darker regions correspond to redder colors in $B-V$. The bluest (lightest) region is H II region 2 of Donahue et al., while other blue knots N of the nucleus of A correspond to H II regions 1, 4, 5 of Donahue et al. (2002, see Fig. 5g). The nuclei of the galaxies are slightly redder regions, while darker regions correspond to dust lanes, especially S of the nucleus of B where various filaments and dust lanes can be seen. There is a dark disk-like feature running SE-NW through the nucleus of B, which may correspond to a disk with a strong absorption lane.

More residual images are shown in Figs. 5c–5e. Figures 5c and d show B residual images of NGC 4410A from the 2.1 m and 0.84 m telescopes, respectively. The most prominent central feature is H II region 2 (Donahue et al. 2002) ∼6″ SE of the nucleus, while there are traces of region 3 to the E, and region 4 is located at the edge of the bright arm structure to the N (compare positions using Fig. 5g). In both Figs. 5c and d, the central regions appear to contain a spiral arm-like structure within a radius of 4–5″, similar in both images. On close inspection, this consists of two radial structures to the NE and SE (that to the SE connects the H II region to the nucleus), plus a curved structure to the W/SW. Tangential features at the ends of these structures appear possibly to be artefacts of the model as they lie on an approximately elliptical shape. Although the appearance of

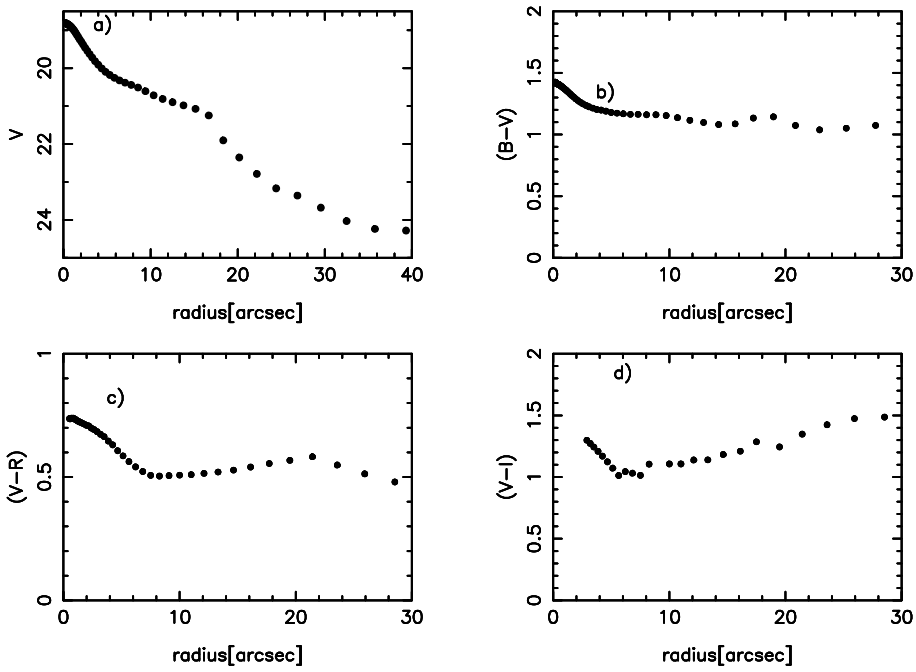

Fig. 8. Surface brightness and color profiles of NGC 4410B **a)** V, **b)** $B-V$, **c)** $V-R$, and **d)** $V-I$. ($1''$ = 470 pc with H_0 = 75 km s^{-1} Mpc^{-1}).

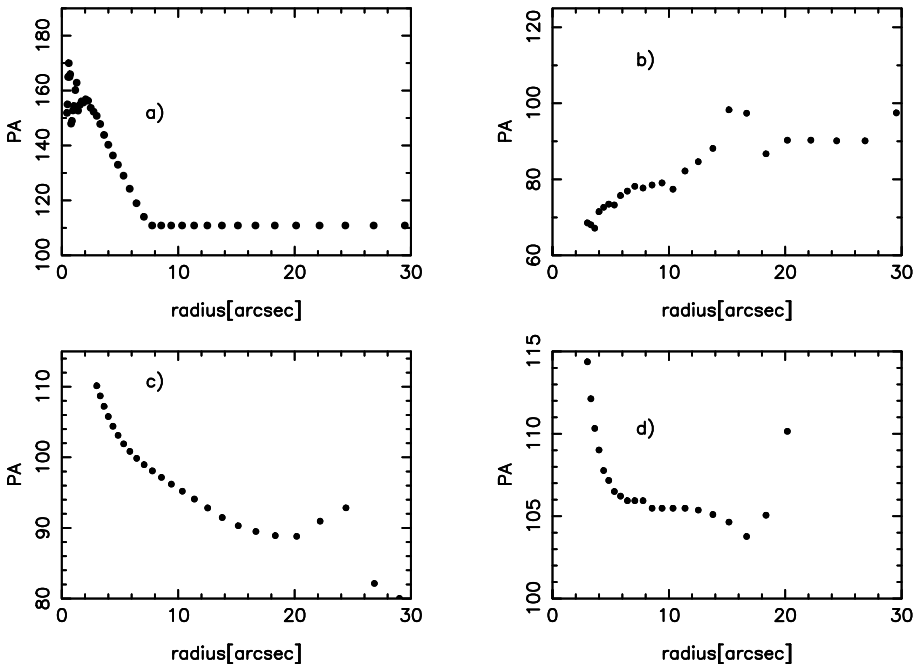

Fig. 9. Position angle versus radius profiles for **a)** NGC 4410A, **b)** NGC 4410B, **c)** NGC 4410C, and **d)** NGC 4410D from the 2.1 m telescope in B band. ($1''$ = 470 pc with H_0 = 75 km s^{-1} Mpc^{-1}).

"internal spiral arms" may be illusory, nevertheless, some of these internal structures may be real. For example, the curved structure to the W connects to another filament, which is directed NW and appears to form part of the NW tidal arm. The residual I images from this telescope do not show the internal structures clearly.

Figure 5e is a residual image of NGC 4410A produced from the HST archive image. The most prominent structure of the lower left is H II region 2 of Donahue et al. (2002), while regions 4, 5, 1 and 6 can all be identified (compare with Fig. 5g), and have their structures revealed in this image. Dust lane structures, especially around region 2, can be traced clearly. The tidal arm to the W and NW can be clearly seen, although the internal structures are not clear.

Figure 5f is an unsharp masked image of NGC 4410A and B in the V band from the 2.1 m telescope. It shows structures similar to those revealed in the $B-V$ color map. The two nuclei are clearly visible as are H II regions 2, 4, 5, 1, and 6 from Donahue et al. (2002), the NW tidal arm and the dust lanes, including the disk-like feature running from SE to NW through the nucleus of B. There is another (previously undetected) knot visible ~4″ NNE of region 2 (also visible in the $B-V$ color map) that does not correspond to a known H II region from Donahue et al. (2002), although it lies adjacent to region 3 (compare with Fig. 5g).

Figure 5g is an image taken from Donahue et al. (2002) in Hα + [N II], which shows the location of the H II regions for reference and easy identification in our figures. Note the arc of

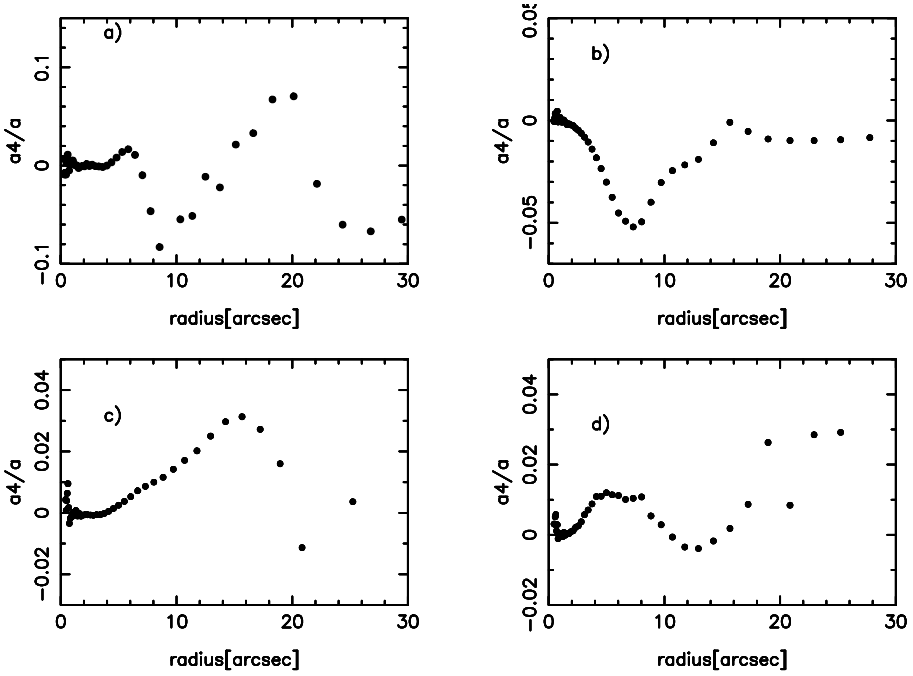

Fig. 10. Profiles of the a_4/a harmonic term versus radius for **a)** NGC 4410A, **b)** NGC 4410B, **c)** NGC 4410C, and **d)** NGC 4410D from the 2.1 m telescope in B band. ($1''$ = 470 pc with H_0 = 75 km s^{-1} Mpc^{-1}).

emission to the NW of the nucleus, which has line ratios indicative of ionization by shocks. It lies further to the NW than those seen in Figs. 5c and d, but may be part of a related structure, connecting the nucleus with the NW tidal arm.

Figure 5h shows our continuum-subtracted Hα + [N II] image of NGC 4410A and B obtained at the 2.1 m telescope at SPM. The poor seeing limits the resolution of the features compared with the Donahue et al. (2002) image (Fig. 5g), but the two nuclei are clearly visible as are H II regions 2, 1, and 4. A possible connection between H II region 2 and the nucleus of NGC 4410A is visible, similar to Fig. 5d.

Figures 6a–d show a V band surface brightness profile of NGC 4410A and $(B-V)$, $(V-R)$, $(V-I)$ color profiles of the same galaxy, respectively. Unlike the surface brightness profiles of the other galaxies reported here, which were produced by ellipse-fitting, these profiles represent the averaged profile on both sides of the galaxy in two radial sectors of width 10 degrees at a position angle of 138° (the apparent major axis), produced using the program SECTOR in ESP (Gray et al. 2000). We use these cuts because, as mentioned in Sect. 2.7, the ellipse-fitting is complicated by the increase in galaxy brightness at 10 arcsec due to a ring of dust just interior to this radius, so the profiles produced by ellipse-fitting may be unreliable outside this radius. Also, the sector profiles are less affeected by uncertainties in the subtraction of the light from galaxy NGC 4410B. In general, the color profiles show a gradient to the blue from the center ($B-V \sim 1.4$) to about $7''$ from the nucleus ($B-V \sim 0.9$) presumably caused by H II region 2 at this radius. Farther out, the $B-V$ and $(V-R)$ profiles remain fairly constant, $(B-V)$ reaching ~1.2 at the extremes of the galaxy. The profile $V-I$ shows more variation, with values in the range 1.2–1.5. Central colors of NGC 4410A imply a population of K or M type stars, while outer colors imply K stars.

More residual images of NGC 4410B in B are shown in Figs. 7a–c. The residual image from the *JKT* in particular (Fig. 7b) shows the approximately axisymmetric SE-NW structure through the center of NGC 4410B mentioned in the discussion of Figs. 5b and f above. This structure may be a galaxy disk with a strong absorption lane, seen edge-on. This structure can also be seen in Fig. 7a (2.1 m telescope), but is not clear in Fig. 7c (84 cm telescope) probably due to the poor seeing. The filament structure in the dust lanes S and E of the nucleus is also seen clearly in these images. The white area to the W is NGC 4410A.

Figures 8a–d show a V band surface brightness profile of NGC 4410B and $(B-V)$, $(V-R)$, $(V-I)$ color profiles. Although color and brightness profiles are again affected by the subtraction of the light from the other galaxy, NGC 4410A, in general, the color profiles are fairly flat apart from having a redder central region (<5 arcsec) from the nucleus.

Figures 9a–b, 10a–b show position angles (PA) and a_4/a profiles for NGC 4410 A and B. For NGC 4410A, these profiles outside a radius of 10 arcsec are unlikely to be reliable, as noted in Sect. 2.7 and earlier in the current section. Within this radius the position angle changes from ~160°, in the nuclear region, to ~110°, at the radius of H II region 2, before adopting a constant value (while we adopt a position angle of 138° for the major axis sector profiles in Fig. 6). The a_4/a profile is slightly disky at 6 arcsec and boxy at 8 arcsec. The galaxy NGC 4410B (Fig. 10b) has boxy isophotes, with values of a_4/a between 0 and −0.05, characteristic of large elliptical galaxies. No disky feature is seen corresponding to the structure oriented SE-NW commented on above, but as this shows up as a darker region, because of absorption, this is not too surprising.

Table 1 contains inclination angles measured at the limiting isophote and the internal extinctions in each band (corrected to face-on, 0° inclination) for each galaxy, calculated as described in Sect. 2.6. Observed and corrected apparent and absolute magnitudes, and observed and corrected global colors of each galaxy are also listed in Table 1. Colors of individual features of the group (knots, bridges and filaments) are listed in Table 2. Except H II region 2 in NGC 4410A, the colors of Table 2 do not have the internal correction for extinction applied (since it is quite difficult to determine to which galaxy each feature corresponds, if any). Note that the surface brightness and color profiles reported above and below have not been corrected for internal extinction.

Table 1. Magnitudes, corrections for internal extinction and global colors for NGC 4410.

Galaxy	NGC 4410A	NGC 4410B	NGC 4410C	NGC 4410D
Morph. type	Sab pec	E?	S0?	SBa
inclination (i)	48.4°	46°	56.24°	48.4°
$A^i_B - A^0_B$ (mag)	0.12	0.11	0.17	0.12
$A^i_V - A^0_V$ (mag)	0.08	0.07	0.12	0.08
$A^i_R - A^0_R$ (mag)	0.06	0.05	0.09	0.06
$A^i_I - A^0_I$ (mag)	0.04	0.03	0.06	0.04
m_B (mag)	14.09 ± 0.06	14.83 ± 0.06	15.49 ± 0.06	15.76 ± 0.06
m^0_B (mag)	13.97 ± 0.06	14.72 ± 0.06	15.32 ± 0.06	15.64 ± 0.06
M_B (mag)	–20.84 ± 0.06	–20.10 ± 0.06	–19.44 ± 0.06	-19.17 ± 0.06
M^0_B (mag)	–20.96 ± 0.06	–20.21 ± 0.06	–19.61 ± 0.06	–19.29 ± 0.06
$(B-V)$	1.13 ± 0.09	1.27 ± 0.09	1.08 ± 0.08	0.94 ± 0.09
$(B-V)_0$	1.09 ± 0.09	1.23 ± 0.09	1.03 ± 0.08	0.90 ± 0.09
$(V-R)$	0.54 ± 0.10	0.65 ± 0.10	0.63 ± 0.09	0.57 ± 0.10
$(V-R)_0$	0.52 ± 0.10	0.63 ± 0.10	0.60 ± 0.09	0.55 ± 0.10
$(V-I)$	1.34 ± 0.10	1.37 ± 0.10	1.74 ± 0.09	1.17 ± 0.10
$(V-I)_0$	1.30 ± 0.10	1.33 ± 0.10	1.68 ± 0.09	1.13 ± 0.10

Table 2. Approximate colors for various regions in the galaxy group NGC 4410. Those for H II region 2 have been corrected for internal extinction.

Object	$(B-V)$ mag	$(V-R)$ mag	$(V-I)$ mag
NW tidal arm	0.73 ± 0.09	0.54 ± 0.09	1.22 ± 0.08
SE filament	1.27 ± 0.31	0.71 ± 0.15	1.39 ± 0.26
H II region 2	0.60 ± 0.09	0.41 ± 0.11	1.05 ± 0.10
knot E	0.49 ± 0.15	0.57 ± 0.09	0.69 ± 0.07
knot F	1.11 ± 0.42	0.44 ± 0.19	1.08 ± 0.27
bridge B-C	1.53 ± 0.24	0.71 ± 0.16	1.41 ± 0.27
bridge C-D	1.71 ± 0.13	0.36 ± 0.04	1.29 ± 0.28

The bluer colors in the NGC 4410A/B interaction are found in the H II regions; region 2 has $(B-V) \sim 0.64$, the NW tidal arm, $(B-V) \sim 0.73$, and knot E (see below), $(B-V) \sim 0.49$. The SE filament has $(B-V)$ colors around 1.2−1.3 i.e., it has a quite red color similar to the nuclei. Within this filament there are two optical knots that were first reported by Hummel et al. (1986), knots E and F. We investigated the area of these knots in the color maps and found that knot E has blue colors ($B-V \sim 0.49$) similar to H II region 2, indicating it may be a site of star formation (although there is no detection of Hα from this region in Donahue et al. 2002 or in the present data). Knot F is only slightly bluer than its surroundings in the SE filament ($B-V \sim 1.1$). The NW filament of NGC 4410A is slightly bluer than the SE filament, by $(B-V) \sim 0.1$, but is also of a generally reddish color and does not have knots of star formation. The colors of the filaments match those of K-type stars.

3.2. NGC 4410C

In Fig. 11, we present images of NGC 4410C. Figure 11a shows a logarithmic image in B from the 2.1 m telescope. Figure 11b is a $(B-V)$ color map (darker appears redder). Figure 11c is a residual image with a complicated structure, but in the center we see three radial arms of length ∼3″. It is unclear whether the "rings" structure at larger radii represents any real structure. In Fig. 11d, the unsharp masked image shows two of the radial structures more clearly to the SE and SW of the nucleus, and these can also be glimpsed faintly on the $(B-V)$ color map (Fig. 11b). Most probably, these faint arms represent a distorted disk structure that is also implied in some images of NGC 4410C. This galaxy is frequently classified as S0. The distortion of the disk may be due to gravitational interaction.

The V band surface brightness profile of NGC 4410C obtained from the 2.1 m telescope is shown in Fig. 12a, while the $(B-V)$, $(V-R)$, and $(V-I)$ color profiles are shown in Figs. 12b–d, respectively. The $(B-V)$ and $(V-R)$ colors are fairly constant with radius (∼1.05 and ∼0.6, respectively), while $(V-I)$ varies between 1.4 and 1.7 in the inner 20″. These are all typical colors for an S0 type galaxy (dominated by K-type stars).

Figure 9c shows the position angle profile of this galaxy and Fig. 10c shows its a_4/a profile. The galaxy NGC 4410C is seen to have $a_4/a > 0$ between about 6 and 18 arcsec from the center, confirming the possibility of a strong disk component between these radii, as indicated by the residual images in Figs. 11c and d.

Details of the bulge-disk decomposition for NGC 4410C are given in Table 3. This contains the disk-to-bulge luminosity ratio (Col. 3), the effective radius of the bulge (Col. 4), the Sérsic index of the bulge (Col. 5), the scale length of the disk (Col. 6), and the colors and face-on corrected colors of the bulge and disk components. The bulge and disk are seen to have similar luminosities and sizes (2−3 kpc), with a best-fitting Sérsic index of around 2.8 for the bulge. The bulge is very red, while the disk is much bluer.

3.3. NGC 4410D

In Fig. 13, we present images of NGC 4410D. The V image in Fig. 13a shows the bar running from ESE to WNW and a faint ring structure at the radius of the extremes of the bar. The $B-V$ color map (Fig. 13b) shows that the bulge has the bluest colors ($B-V \sim 0.5$), while the area of the bar and ring has $B-V$ between 0.5−1.0 and the rest of the galaxy has $(B-V) \sim 1$. The residual image in B (Fig. 13c) shows the bar structure clearly on either side of the center, and on both sides the bar is seen to curve to the north, implying a distortion that may be caused by the gravitational interaction between the galaxies (Hummel et al. 1986). This distorted bar is clearly seen in all the residual images in Fig. 4. In the unsharp masked image (Fig. 13d) a similar distortion of the bar is seen, also traces of the ring-like structure at the extremes of the bar, which probably represents two short faintish tightly-wound spiral arms, consistent with the SBa classification. This ring-like (arm-like) structure is seen also in our (Hα + [N II]) image (Fig. 13e). Our (Hα + [N II]) image is not calibrated but NGC 4410A and NGC 4410D are in the same

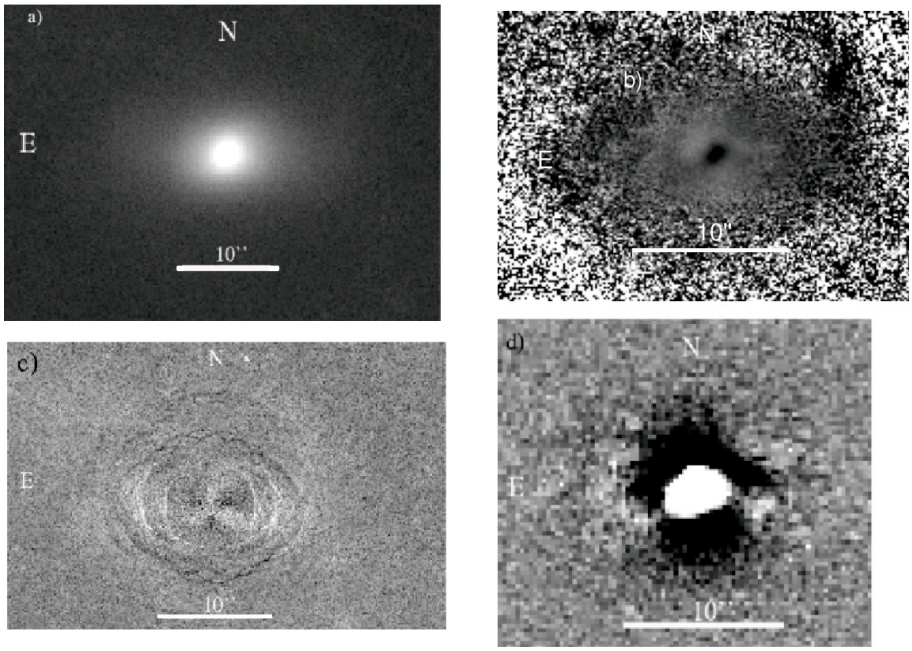

Fig. 11. NGC 4410C in **a)** a logarithmic image in B, **b)** a $(B-V)$ color map image, **c)** a residual image, and **d)** an unsharp masked image from the 2.1 m telescope. ($1''$ = 470 pc with H_0 = 75 km s^{-1} Mpc^{-1}).

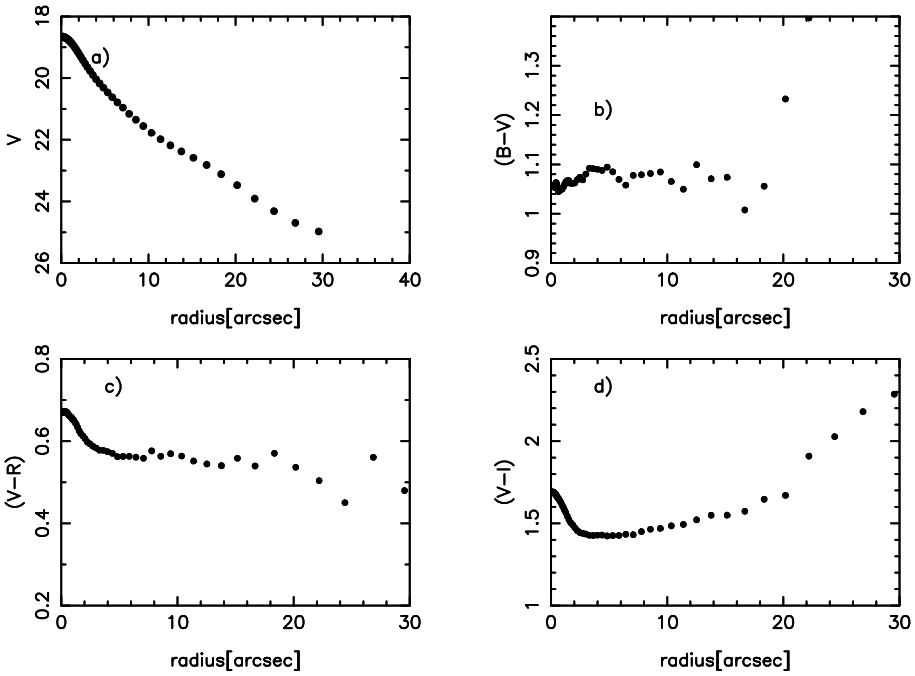

Fig. 12. Surface brightness and color profiles of NGC 4410C **a)** V, **b)** $B-V$, **c)** $V-R$, and **d)** $V-I$. ($1''$ = 470 pc with H_0 = 75 km s^{-1} Mpc^{-1}).

CCD image and we have calibrated the (Hα + [N II]) flux, relatively, with the results of Donahue et al. (2002) for NGC 4410A, and we have measured flux in counts in various parts of our CCD image with the *phot* task with different apertures. We found that the total flux of the NGC 4410D nucleus is $\sim 6.2 \times 10^{40}$ erg s^{-1}, while the total flux in the surrounding disk is $\sim 3.5 \times 10^{40}$ erg s^{-1}. The total is about 70% of the flux of (Hα+[N II]) of NGC 4410A measured by Donahue et al. (2002), implying that NGC 4410D may have a SFR of 0.7–3 $M_\odot$ yr^{-1}.

The V band surface brightness profile of NGC 4410D is shown in Fig. 14a. Figure 14b displays the $(B-V)$ color profile of this galaxy, confirming the trend shown in Fig. 13b of a blue central part of the bulge ($B-V \sim 0.5$), with the color becoming steadily redder with radius until it reaches $B-V \sim 0.9$ at $r \sim 9$ arcsec. Further out, the galaxy becomes bluer by 0.1–0.15 (at the radius of the ring/arms), then becomes redder again. The central colors of the bulge and bar region are those of G type stars. Figure 14c shows the $(V-R)$ color profile, which remains generally constant around a value of ~0.5.

Figure 9d contains the position angle profile of this galaxy while its a_4/a profile is shown in Fig. 10d. The a_4/a profile shows that the galaxy is disky within 10 arcsec of the center and beyond 18 arcsec from the center, and in between it has boxy isophotes (the isophotes are dominated by the bar at these intermediate radii).

The bulge-disk decomposition for NGC 4410D shows that the disk component, although large, is somewhat underluminous (D/B ratios are around 0.6), while the scale length of the disk (4 kpc) is twice the effective radius of the bulge. The Sérsic index of the bulge is around 1.2. The bulge component is significantly bluer than the disk, implying that most of the star formation is in a nuclear starburst.

Table 3. Details of bulge-disk decomposition for NGC 4410C and D.

Galaxy	Band	D/B	r_e (kpc)	n	r_d (kpc)	$(B-V)_b$	$(B-V)_d$	$(B-V)_b^0$	$(B-V)_d^0$
NGC 4410C	*B*	1.4	2.7	2.6	2.1	1.36	0.88	1.31	0.83
	V	0.9	3.2	2.8	2.0				
	R	1.0	3.2	2.9	2.0				
NGC 4410D	*B*	0.6	2.3	1.46	4.1	0.87	1.04	0.83	1.00
	V	0.7	2.2	1.15	3.7				
	R	0.6	2.3	1.18	3.5				

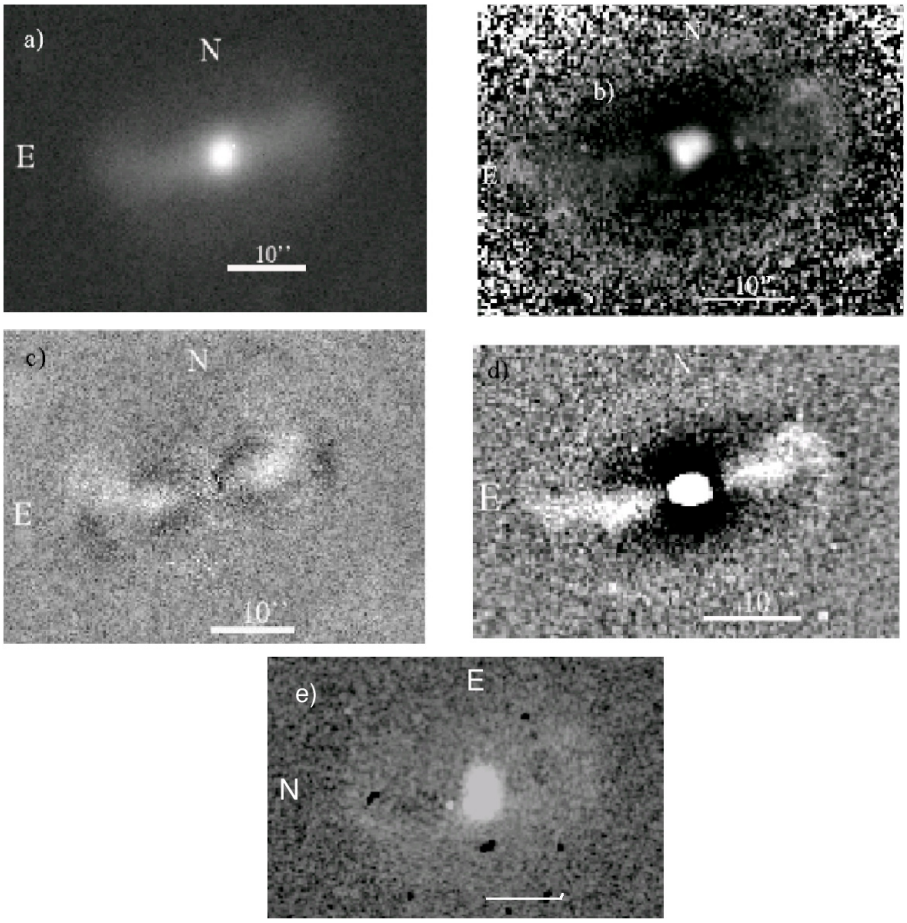

Fig. 13. NGC 4410D in **a)** a logarithmic image in *B*, **b)** a $(B-V)$ color map image, **c)** a residual image in *B*, **d)** an unsharp masked image, **e)** (Hα + [N II]) image, all from the 2.1 m telescope. ($1''$ = 470 pc with H_0 = 75 km s^{-1} Mpc^{-1}).

3.4. The optical bridges

The optical bridges between NGC 4410A/B and NGC 4410C, and between NGC 4410C and D, tend to have very red colors, corresponding to K and even M stars. The bridge between NGC 4410A/B and C has a $(B-V)$ color of ~1.5, while the bridge between NGC 4410C and D has $(B-V) \sim 1.7$. This bridge between NGC 4410C and D is divided into a bright region to the N, of dimensions 1.7 × 0.2 arcmin and a fainter region, parallel and contiguous with the bright region, to the S, of dimensions 1.7 × 0.3 arcmin. This distinction between the two regions is most clear in the deepest image, that of the digitally co-added Schmidt data (see Figs. 1 and 2).

The bridge between NGC 4410A/B and C has typical *B* surface brightnesses of 24.5–25.3 mag arcsec^{-2}, while that between NGC 4410C and D is somewhat brighter, 23.8–24.7 mag arcsec^{-2}.

3.5. Geometry of system

Tschöcke et al. (1999), from inspection of the HST image of NGC 4410A, considered that this galaxy was in an almost face-on orientation (low angle of inclination). However, the evidence from the axis ratio in our ellipse-fitting suggests that it is at an angle of ≈45°. The galaxies NGC 4410B and D seem to lie at similar angles, while NGC 4410C is more inclined to the line-of-sight at ≈56°. So all the galaxies appear to be at an intermediate elongation.

The bridges between galaxies are quite elongated, especially that between C and D, suggesting that they lie mainly in the plane of the sky. So we seem to be observing this group of four galaxies at a favorable orientation in which the major axis of the group is close to being in the plane of the sky. The major axes of NGC 4410B, C, and D also seem to be close to the major axis of the group (<30° from this axis), while the major axis of NGC 4410A is approximately perpendicular to that of the group.

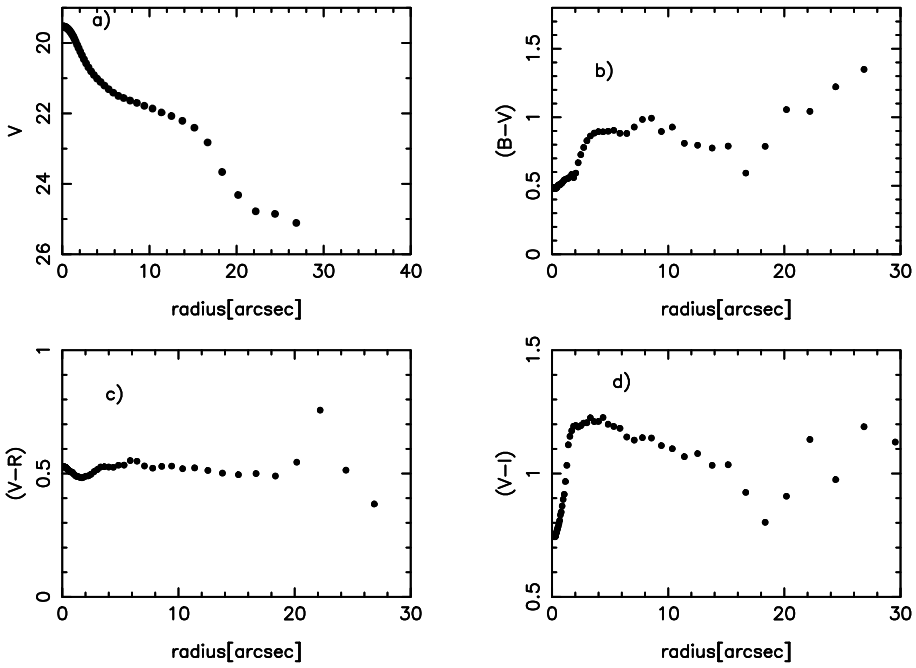

Fig. 14. Surface brightness and color profiles of NGC 4410D **a)** V, **b)** $B-V$, **c)** $V-R$, and **d)** $V-I$. ($1'' = 470$ pc with $H_0 = 75$ km s^{-1} Mpc^{-1}).

4. Discussion

4.1. Colors and stellar populations of the NGC 4410 group.

The global colors of the galaxies lie in the range $(B-V) \sim 0.9-1.3$, corresponding to red giant stars of type K0–K2. In general, the nuclei are slightly redder than the other parts of the galaxies, apart from NGC 4410D, which has a nucleus 0.5 mag bluer than the outer-bulge region, and a bar and short spiral arms with star formation and colors similar to those of the nucleus, before the outer galaxy turns redder. However, with the high resolution (better seeing) of the La Palma data, the most central regions of the nucleus of NGC 4410D are seen to be redder than the blue "inner bulge" region.

We use the models of Bressan et al. (1994) to get more detailed information for the early-type galaxies NGC 4410B and NGC 4410C, and the bulge of NGC 4410D. For NGC 4410C, the face-on corrected $(B-V)_0$ of 1.03 would imply a stellar population with age $10-15 \times 10^9$ years for solar metallicity ($Z = 0.02$) and age $3-6 \times 10^9$ years for high metallicity ($Z = 0.05$). The bulge-disk decomposition of NGC 4410C gives a corrected color of $(B-V)_0 \approx 1.31$ for the bulge, but this is redder than any model of Bressan et al. (1994), implying that more internal extinction may be present. For NGC 4410B, with face-on corrected color of $(B-V)_0 \approx 1.23$, the only model that corresponds to this has $Z = 0.05$ and age of stellar population of $\sim 20 \times 10^9$ years, also suggesting we are underestimating internal extinctions. The other "early-type" component that we can isolate in the group is the bulge of NGC 4410D, of corrected color $(B-V)_0 \approx 0.83$, which clearly contains a young population, of possible ages $2-3 \times 10^9$ years ($Z = 0.02$), $3-6 \times 10^9$ yr ($Z = 0.008$), and $6-9 \times 10^9$ yr ($Z = 0.05$).

We use the starburst models of Bruzual & Charlot (2003) to interpret the colors for the late-type galaxies NGC 4410A and NGC 4410D and the disk component of NGC 4410C. For NGC 4410C, the face-on corrected color of the disk component is $(B-V)_0 \approx 0.83$, which implies a age of $\sim 10^9$ years for a high-metallicity population ($Z = 0.05$) and $\sim 2 \times 10^9$ yr for $Z = 0.02$.

For NGC 4410D, the face-on corrected global color is $(B-V)_0 \approx 0.90$ which implies an age of $\sim 3 \times 10^9$ years for a high-metallicity population ($Z = 0.05$) and $\sim 10^{10}$ yr for $Z = 0.02$. The color of the disk component is redder, $(B-V)_0 \approx 1.00$, as more recent star formation seems to have taken place in the center, and the implied ages are $\sim 3 \times 10^9$ yr for $Z = 0.05$ and $\sim 2 \times 10^{10}$ yr for $Z = 0.02$.

NGC 4410A has a global corrected colour of $(B-V)_0 \approx 1.09$, implying a population at least as old as 2×10^{10} years even for a high metallicity ($Z = 0.05$).

The optical knot E, the H II regions, and the nucleus and ring in NGC 4410D, have colors in the range $(B-V) \sim 0.5-0.7$. Using the models of Bruzual & Charlot (2003), this colour range corresponds to an age range of $0.5-1.2 \times 10^9$ years for a high ($Z = 0.05$) metallicity population, $0.65-1.5 \times 10^9$ years for a normal ($Z = 0.02$) metallicity population and $0.8-3.0 \times 10^9$ years for a low ($Z = 0.008$) metallicity population. The optical bridges appear to have very red colors $(B-V) \sim 1.5-1.7$, while the tails of NGC 4410A/B have $(B-V) \sim 1.1-1.3$. Hence, there is no evidence for recent star formation in the tails, in fact, the colors are too red for almost all the models.

The knot E has blue colors, but is not detected in (Hα+[N II]) in our data nor in the data of Donahue et al. (2002), while the knot F has similar colors to the rest of the galaxy and does not appear to be a region of star formation. Knot E is also detected at radio wavelengths (Hummel et al. 1986) and so may be associated with optical synchroton emission (Donahue et al. 2002). Estimating a R magnitude of ~ 19 gives an optical to 4.9 GHz spectral index (α) of approximately -0.31 (Donahue et al. 2002), while the 4.9 and 1.5 GHz flux densities give an α of -0.47 ($L_\alpha \propto \nu^\alpha$, Donahue et al. 2002). Our $(B-V)$ color of ≈ 0.5 for the knot would imply a spectral index of ~ -1.5, while our $(B-I)$ color of ~ 2.1 would give a spectral index of around -2.5 over the wider wavelength interval between B and I. Thus, our optical data is inconclusive as to whether this may represent synchrotron emission or not, giving a widely varying spectral index, while Donahue et al. (2002) point out that the upper limit for detection of Hα emission is well above the Hα luminosities of H II regions in the tails of various galaxies, including the possible jet-induced H II regions in Cen A (Graham 1998). So an identification of the knot E as a H II region remains probable.

Overall, in these galaxies, there seems to be no great evidence for recent star formation apart from in the H II regions of NGC 4410A and perhaps in knot E, and the nucleus, bar and ring/arms of NGC 4410D, which, according to its relative Hα + [N II] flux, is about 70% as active as NGC 4410A in terms of star formation. Most of the reported colors imply ages of stellar populations between 3×10^9 and 3×10^{10} years. The minimum age compatible with observed colors is 5×10^8 years for high-metallicity populations in knot E, H II region 2, and the bulge of NGC 4410D. Given that the normal dynamical timescale for galaxy interactions is of the order of $\sim10^8$ years, these reported ages do suggest that the processes of interactions and mergers in this group are taking place over a much longer timescale (or maybe that the current dominant members of the group have already experienced at least one major merger). In any case, the evoutionary processes in the group (and star formation stimulated by these processes) appear to be playing out over a very long timescale.

4.2. Morphological classification

The galaxies NGC 4410A and B are very difficult to classify accurately because of the strong interaction they are currently undergoing. For NGC 4410A, because of the presence of H II regions, tidal arm, and dust, we have no reason to doubt the Sab pec classification previously given. For NGC 4410B, the possible presence of a dust lane or dusty disk at a position angle of $\sim$135° (SE-NW), together with the boxy isophotes, and relatively bright absolute magnitude, may mean that this galaxy is a giant elliptical galaxy with an embedded dusty disk comparable to Cen A.

NGC 4410C has been classified as an E or an S0 type galaxy. It has the typical $r^{1/4}$ profile of an elliptical galaxy (not shown), but in the unsharp-masked image it appears to show a distorted disk, indicating that it is more probably of lenticular type. The bulge-disk decomposition also confirms the presence of a disk, containing 50% of the luminosity of the galaxy, and of much bluer color, implying that this galaxy may have a morphological type of S0 or even Sa.

The bar of NGC 4410D also appears to be distorted by the interaction, and we find blue colors in the centre of D, along with a bluish ring/spiral arms and bar, suggesting the possible presence of a nuclear starburst in this galaxy, with gas funneled to the central regions by the bar. The overall morphology of NGC 4410D is consistent with the SBa classification cited previously, if the "ring" is interpreted as two short, tightly-wound spiral arms. The disk-bulge decomposition is affected by the presence of the bar and by the increase in luminosity of the bulge due to the inferred nuclear starburst, but we note that the disk does appear to be a thin, underluminous structure. Apart from NGC 4410A, NGC 4410D was the only other of these four galaxies to be detected in H I and CO, with $M_{\rm H\,I} \sim 5 \times 10^8\ M_\odot$ and $M_{\rm H_2} \sim 8 \times 10^8\ M_\odot$ (Smith 2000). Its H I exists in two spatially and kinematically distinct parts, one near the optical velocity at 6960 km s^{-1} and associated with the main disk and a northern extension (this velocity also corresponds to the CO detection), and the other $\sim$400 km s^{-1} more positive, associated with a southern tail which points toward NGC 4410F (Smith 2000). The blue colors of the arms and bar are centered on the nucleus of the galaxy and so would seem to be associated with the lower velocity component.

In their study of star formation in NGC 4410A, Donahue et al. (2002) concluded that this galaxy has moderate star formation of around 1–4 $M_\odot$ per year. We find the blue colors associated with recent star formation only in the H II regions and knot E, and so this seems to be in agreement with a moderate star formation rate. The extensive regions with blue colors in the center, bar and ring/arms of NGC 4410D seem likely to be associated with a SFR about 70% as high and with nuclear starburst phenomena, and the two distinct kinematic systems in H I may indicate that some type of merger of NGC 4410D with a H I cloud is taking place.

4.3. The residual structures

While real galaxies may have either disky or boxy isophotes (Binney & Merrifield 1998), the isophotal models generated by *ellipse* (IRAF) produce perfect ellipses in such a way that if we subtract these models from an image of a galaxy with disky isophotes, the residual image might show up axisymmetrical linear structures. On the other hand, NGC 4410D (Fig. 13c) seems to have a symmetrical bar as a result of the subtraction. It is clear that this is a real bar (Hummel et al. 1986; Smith 2000; Smith et al. 2003) and in our Fig. 13a. We note blue colors due to star formation and the distortion of the bar due to gravitational interactions (as mentioned in Hummel et al. 1986) in our images (Fig. 13).

The optical structures seen in NGC 4410A (Figs. 5c and 5d) show coincidence with H II regions east, SE, and NE of the nucleus. Barazza et al. (2002), in their search for evidence for spiral and bar features in early-type dwarf galaxies, noted that such disk signatures could be caused by specific behaviors of the position angle and ellipticity profiles, mimicking spiral structure although no such structure genuinely exists. They resolve this ambiguity by also using an unsharp masking technique.

Grützbauch et al. (2005) perform subtraction of isophotal models to produce residual images of galaxies in the NGC 4756 group. The galaxy IC 829 shows four faint radial structures unlikely to be real. For MCG-2-33-36, the subtracted model image shows a complex system of three long spiral arms, two of which start from the nucleus. In the same group is MCG-2-33-35, in which the residual image reveals the existence of two open arms that depart from a bar.

Having such contrasting results, the unsharp masking process becomes crucial in unveiling and confirming the existence of hidden structures, as in Barazza et al. (2002). Even when the internal arms of NGC 4410A appear as an asymmetrical structure surrounding the nucleus, they may not be real as they are absent from the unsharp masked image (Fig. 5f). The structure that extends to the NW in Fig. 5d may be an internal part of the NW tidal arm.

5. Summary and conclusions

We observed the NGC 4410 group of galaxies with the 2.1 m and 0.84 m SPM telescopes and the 1.0 m telescope from La Palma, in the *BVRI* Johnson, *BRI* Johnson-Cousins, and *BVRI* Harris filters, respectively. Our residual images of NGC 4410A from the 2.1 m amd 0.84 m telescopes revealed what appear to be internal "spiral arm-like" structures, however, the unsharp masked image from the 2.1 m telescope suggests that such structure may not be real. According to the obtained colors (corrected for internal extinctions to face-on inclination), there are few areas with active star formation in this group. The bridges and tails, and most parts of the galaxies, have very red colors. Some exceptions are found in NGC 4410A: the H II regions and knot E, which have bluer colors than the rest of this galaxy. Knot E

could possibly be a hot spot of optical synchrotron emission, but the spectral indices derived from our optical colors do not agree with the optical-radio spectral indices of Donahue et al. (2002), so it may be more likely that it is a H II region. However, NGC 4410D has a blue nucleus, bar, and spiral arms/ring suggesting it is currently very active in terms of star formation processes, its Hα emission is 70% of that of NGC 4410A. It may be currently merging with a H I gas cloud, and has two kinematically distinct systems. The galaxy NGC 4410D also has a bridge connecting it with NGC 4410C and its H I gas is oriented toward NGC 4410F (Smith 2000). It is not clear which galaxy or cloud has provoked the current burst of star formation.

The galaxy NGC 4410B has a linear structure running diagonally SE-NW through its center which shows up as a red feature in the $(B - V)$ image and a dark feature in the unsharp-masked and residual image. This could be an edge-on disk with a strong absorption-lane feature, or even a distorted red bar. The isophotes of this galaxy are boxy, (as the disk appears as an area of absorption), so NGC 4410B may be a giant elliptical galaxy comparable with Cen A in having an embedded dusty disk.

NGC 4410C appears to be confirmed as a lenticular galaxy from our results. A distorted disk-like structure is seen in the unsharp-masked and residual images, the isophotes are disky, and the bulge-disk decomposition implies that the disk feature has a similar luminosity to the bulge.

In general, this small group of gravitationally-interacting galaxies is currently in a relatively tranquil evolutionary state in terms of star formation, apart from NGC 4410D and the H II regions in NGC 4410A. The minimum age of stellar populations suggested by the observed colors is around 5×10^8 years while most ages are between 3×10^9 and 3×10^{10} years, long compared with the "dynamical timescale" of 10^8 years. Galaxies NGC 4410A and B are currently merging and it is thought likely that eventually NGC 4410C and D will merge with the subsequent product, forming an elliptical galaxy (Smith 2000). Other authors, e.g. Moles et al. (1994) have found that star formation in compact groups of galaxies (Hickson Compact Groups) is not higher than in isolated pairs of galaxies, and that the timescales for mergers to occur seem to be long in these groups. They find no galaxies with global starbursts, but do not exclude the possibility of nuclear starbursts. Our results for the NGC 4410 group seem to be compatible with these conclusions, as we find star formation only in the H II regions of NGC 4410A and a possible nuclear starburst in NGC 4410D, and ages of populations implying a long timescale for the interaction and mergers. (The NGC 4410 group has a compact core including the four galaxies in interaction, but is not classified as a Hickson Compact Group because of the contamination of foreground Virgo cluster members). We suggest carrying out detailed individual studies of other groups of galaxies to further investigate the conclusions of Moles et al. (1994).

Acknowledgements. We thank an anonymous referee for making many, very helpful, suggestions. We thank PROMEP for providing financial help for the project "Research into the nature of faint light in clusters of galaxies" under its program "Help in the incorporation of new, full-time lecturers", which aids researchers in state universities in Mexico. We thank the staff of the UKST for obtaining the Schmidt films between 1991 and 1994, the APM group for scanning the films, and Mike Irwin for helpful advice. The co-addition of the APM scans of the Schmidt films was carried out at the Manchester STARLINK node with the help of Dave Berry. We also thank all the staff in La Palma y San Pedro Martir for all their technical support. Pérez Grana acknowledges support from CONACyT (México) grant 193057. E.d.l.F. acknowledges financial support from CONACyT (México) grant 124449. We thank Megan Donahue for permission to reproduce one of her figures. Special thanks to Andrés Rodríguez for computer management and software help and to Miguel Chávez for useful discussions.

References

Barazza, F. D., Binggeli, B., & Jerjen, H. 2002, A&A, 391, 823
Binney, J., & Merrifield, M. 1998, Galactic Astronomy (Princeton: Princeton University Press)
Bressan, A., Chiosi, C., & Fagotto, F. 1994, ApJS, 94, 63
Bruzual, G., & Charlot, S. 2003, MNRAS, 344, 1000
Chiba, M., & Yoshi, Y. 1995, ApJ, 442, 82
Donahue, M., Smith, B., & Stocke, J. 2002, AJ, 123, 1922
Graham, J. A. 1998, ApJ, 502, 245
Gray, N., Taylor, M., & Privett, G. 2000, ESP-Extended Surface Photometry, ver. 0.10-8 User's Manual, Starlink, Chilton, Rutherford Appleton Lab.
Grützbauch, R., Kelm, B., Focardi, P., et al. 2005, AJ, 129, 1832
Hummel, E., Kotanyi, C. G., & van Gorkom, J. H. 1986, A&A, 155, 161
Katsiyannis, A. C., Kemp, S. N., Berry, D. S., & Meaburn, J. 1998, A&AS, 132, 387
Katsiyannis, A. C., Kemp, S. N., Berry, D. S., & Meaburn, J. 2001, Ap&SS, 276, 733
Kemp, S. N., & Meaburn, J. 1993, A&A, 274, 19
Kemp, S. N., Katsiyannis, A., Meaburn, J., Chavez, M., & Berry, D. S. 2002, RMxAC, 14, 70
Kemp, S. N., de la Fuente, E., Franco-Balderas, A., & Meaburn, J. 2005, ApJ, 624, 680
Khosroshahi, H. G., Wadadekar, Y., & Kembhavi, A. 2000, ApJ, 533, 162
Landolt, A. U. 1992, AJ 104, 430
Matthews, L. D., van Driel, W., & Gallagher, J. S., III 1998, AJ, 116, 2196
Moles, M., del Olmo, A., Perea, J., et al. 1994, A&A, 285, 404
Pierini, D. 1999, A&A, 352, 49
Smith, B. J. 2000, ApJ, 541, 624
Smith, B. J., Nowak, M., Donahue, M., & Stocke, J. 2003, AJ, 126, 1763
Sparke, L., & Gallagher, J. 2000, Galaxies in the Universe (Cambridge: Cambridge University Press)
Tschöcke, D., Hensler, G., & Junkes, N. 1999, A&A, 343, 373
Tully, B., & Fouqué, P. 1985, ApJS, 58, 67